Electronic Supplementary Material (ESI) for Nanoscale.
This journal is © The Royal Society of Chemistry 2022

Centimetre-scale single crystal α-MoO_3: oxygen assisted self-standing growth and low-energy consumption synaptic devices

Xin Shan[a,b], Zeyu Wu[b], Yangyang Xie[b†], Xin Lin[b], Baozeng Zhou[b], Yupeng Zhang[b], Xiaobing Yan[c], Tianling Ren[d], Fang Wang[b†], Kailiang Zhang[b†]

[a] *School of Materials Science and Engineering, Tianjin University of Technology, Tianjin 300384, China*

[b] *Tianjin Key Laboratory of Film Electronic & Communication Devices, School of Integrated Circuit Science and Engineering, Tianjin University of Technology, Tianjin 300384, China*

[c] *College of Electronic and Information Engineering, Hebei University, Baoding 071000, China*

[d] *School of Integrated Circuits and Beijing National Research Center for Information Science and Technology (BNRist), Tsinghua University, Beijing 100084, China*

During CVD growth of α-MoO_3 nanosheets, oxygen was introduced into the reaction chamber. It promotes rapid growth of the nanosheets along the c-axis (001) to the centimeter level. With pure Ar as carrier, Mo has three valence states: binding energies of 229.8 eV and 232.3 eV to the Mo^{4+}, 231.6 eV (Mo $3d_{5/2}$), 234.9 eV (Mo $3d_{3/2}$) to the Mo^{5+}, 233.2eV (Mo $3d_{5/2}$) and 236.3eV (Mo $3d_{3/2}$) to the Mo^{6+}. However, when 18% O_2 was introduced into the tube, the Mo^{6+} was the dominant that illustrated less oxygen vacancy (V_o) defects, as shown in Fig. S1.

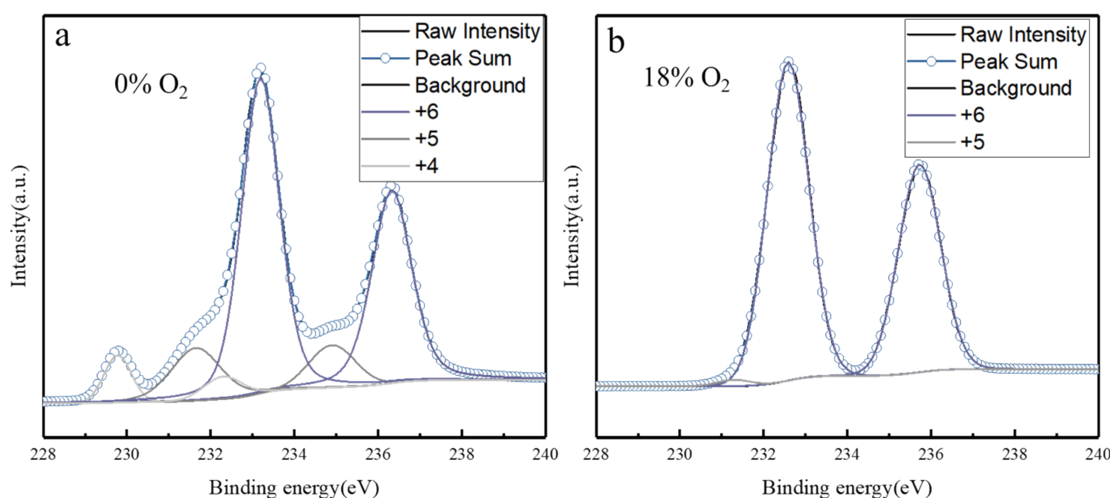

Figure S1 X-ray photoelectron spectroscopy of Mo 3d of α-MoO_3 nanosheet: (a) Pure Ar as carrier gas and (b) Carrier gas consisting of 18% O_2 and 82% Ar.

The a, b, c of Fig. S2 are AFM topographic images corresponding with 6%, 12% and 18% oxygen partial pressure (the percentage of oxygen flow in the total carrier gas flow) during growth process, and their thicknesses are 800nm, 320nm and 200nm, respectively. Moreover, the thickness decreased with increasing oxygen partial pressure. According to periodic bond chain theory, it can be speculated that increasing of oxygen concentration accelerates the growth of α-MoO_3 nanosheets in the direction of stronger bonding energy (along [001]), which restricts the growth in the vertical direction (along [010]).

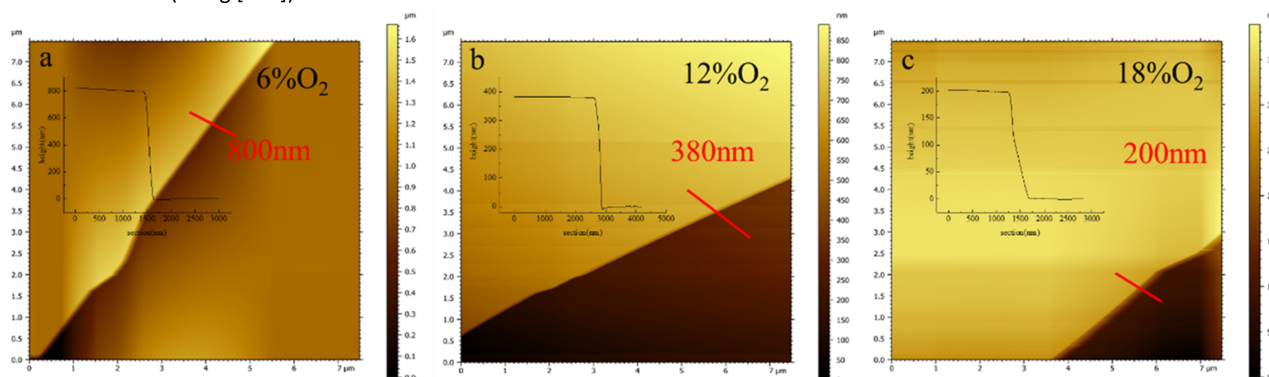

Figure S2 The thickness of α-MoO_3 nanosheets: (a-c) are α-MoO_3 nanosheets topographies of 6%, 12%, 18% oxygen partial pressure, respectively. The inset is corresponding thickness

measurement.

The topographies of both α-MoO_3 and Ti electrode layers were characterized by an atomic force microscope (in topography mode). From the topography of E-beam evaporation, a 50 nm thickness Ti film is shown in Fig. S3(a) and (b). The atomic force microscopy (AFM) results showed the good uniformity of the deposited Ti electrode. The root-mean-square surface roughness of Ti electrode is 0.79 nm, which is beneficial to construct Ti/α-MoO_3 heterointerface.

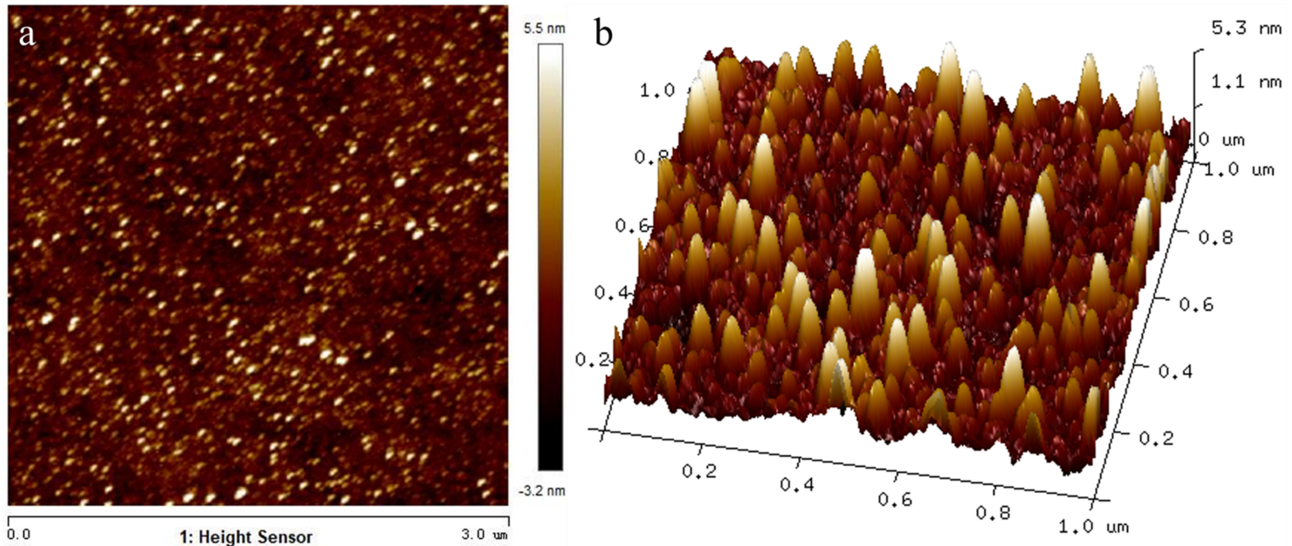

Figure S3 (a) 2D topography of Ti electrode. (b) 3D topography of Ti electrode.

To further investigate the effect of the oxygen partial pressure on the devices, the α-MoO_3 nanosheets were exfoliated to similar thickness (~145 nm) for the fabrication of the devices. The topography image of Ti/α-MoO_3 hybrid structure and the thickness of α-MoO_3 layer are shown in Fig. S4.

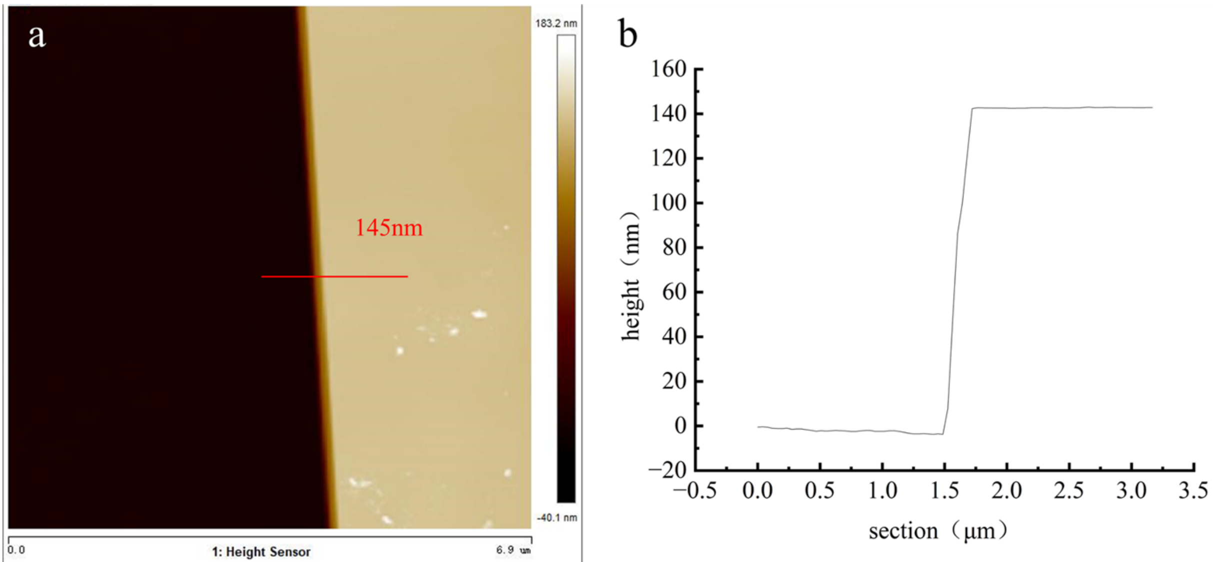

Figure S4(a) The AFM topography of exfoliation α-MoO_3 nanosheets. (b) The thickness measurement of red line is drawn in (a).

The α-MoO_3 memristor at LRS when voltage sweeps from +2V to 0 V. When the α-MoO_3 was grown under 6% and 12% oxygen partial pressure, their slopes of double-logarithmic fitted curve were nearly 1 at LRS of the α-MoO_3 memristors, as shown in Fig. S5(a) and (b). It indicates that the trap is filled with injection carriers. When the oxygen partial pressure came to 18%, the slopes of double-logarithmic fitted curve exhibited 1.28 and 0.96, as shown in Fig. S5(c). It indicates that the traps remain unfilled at high voltage region and then gradually filled. Under the 18% oxygen partial pressure, both the LRS and HRS of α-MoO_3 memristor followed SCLC conductive mechanism.

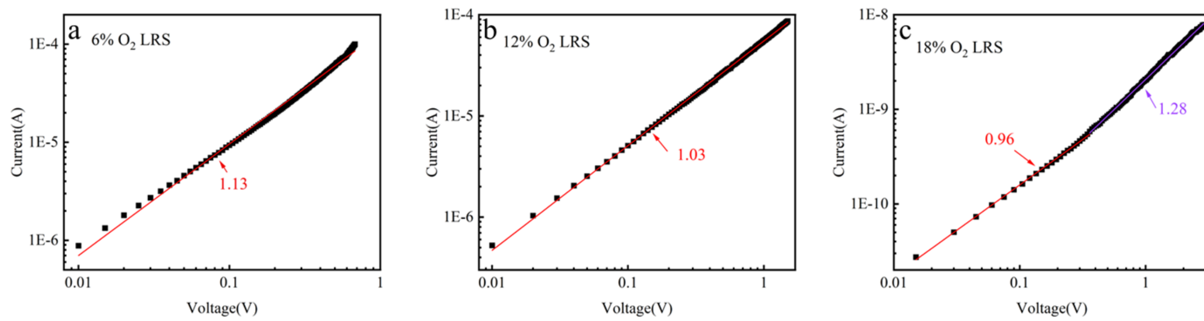

Figure S5 Double-logarithmic fitting results of the α-MoO_3 memristor at LRS: (a-c) are α-MoO_3 memristors prepared at oxygen partial pressure of 6%, 12% and 18%.

To further investigate the Ti/α-MoO_3 interfacial contact properties, XPS depth profile analysis was used to characterize the Ti/α-MoO_3 heterostructure shown in Fig.S6. An energy of 2 keV was used to etch the α-MoO_3 nanosheet to investigate the valence of elements at the Ti/α-MoO_3 interface.

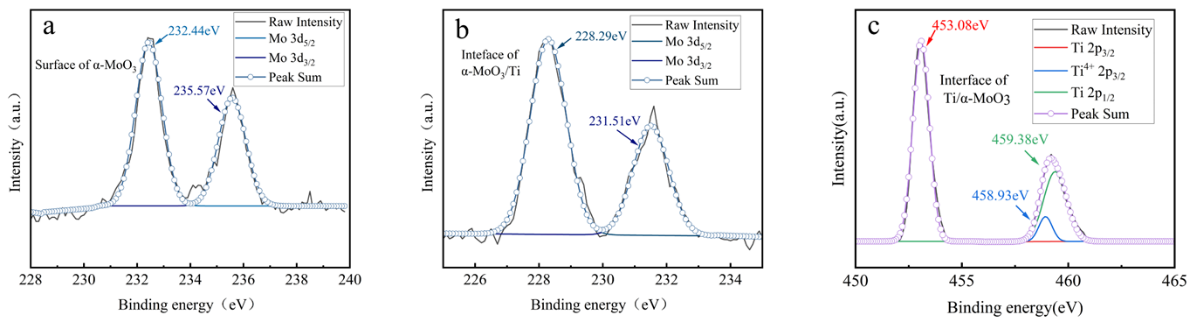

Figure S6 XPS spectra of (a) Mo 3d on the surface of Ti/α-MoO_3 heterostructure. (b) Mo 3d at the heterogeneous interface after etching. (c) Ti 2p at the Ti/α-MoO_3 heterogeneous interface after etching.

The synaptic tunability can be emulated by the α-MoO_3 memristor. Fig. S7 shows the analog switching of the memristor under excitation voltage pulses.

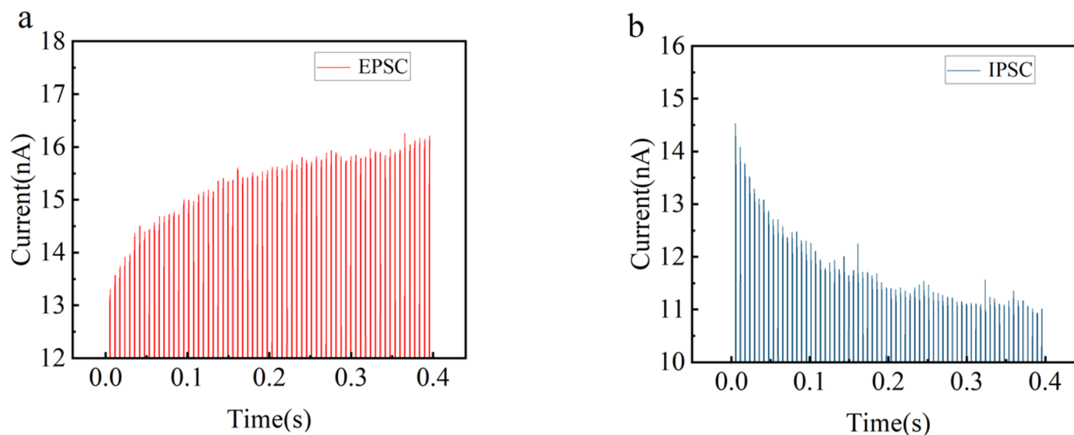

Figure S7 The current-time curve of α-MoO_3 memristor: (a) EPSC triggered by consecutive by voltage pulses with +3 V and 1ms width. (b) IPSC triggered by consecutive by voltage pulses with -3 V and 1ms width.

The spike amplitude-dependent plasticity (SADP) is one of the fundamental behaviors of biological synapses. With different amplitudes (2.5, 5 and 6 V), a successive voltage pulses were applied on the memristor shown in Fig. S8 (a). The ratio of weight change was defined as

$$weight\ change\ ratio = ((G_n - G_0)/G_0)\ \times 100\% \quad (1)$$

where G_0 is the initial conductance, G_n is conductance after the action voltage of the nth pulse. In this device, the ratio of weight change significantly

varies with pulse amplitude, which is similar with the observed in biological excitatory synapses. Spike rate-dependent plasticity (SRDP) as an important part of Hebbian learning rules that also is one of the basic working mechanisms of learning. Therefore, the excitation voltage was applied to pre-synapse (top electrode) with a total time of 0.5 s, an amplitude of +8 V, a pulse width of 10ms and different pulse intervals. The weight sharply increases when presynaptic signal frequency exceeds a certain threshold (0.16 kHz), which exhibits high-pass filtering, as shown in Fig. S8 (b).

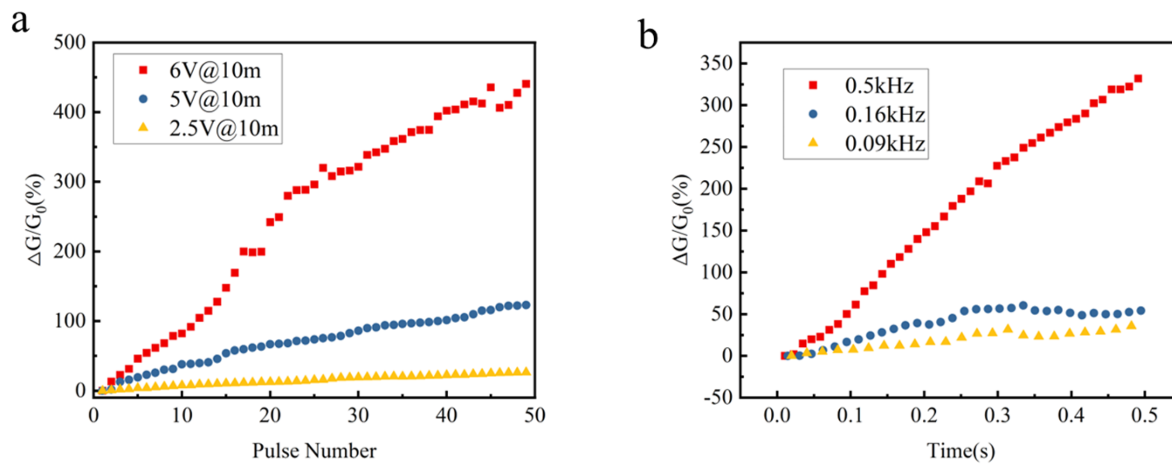

Figure S8 (a) SADP of α-MoO_3 memristor conductance change ratio triggered by a series of excitation pulses with the same duration time (10 ms) and different amplitudes (2.5, 5, and 6 V). (b) The α-MoO_3 memristor SRDP performance under variable frequencies excitation pulses at 8 V and 10 ms.